Journal of
Synchrotron Radiation
ISSN 0909-0495

Received 12 February 2004
Accepted 21 November 2005

Single-bounce monocapillaries for focusing synchrotron radiation: modeling, measurements and theoretical limits

Rong Huang[a]*‡ and Donald H. Bilderback[a,b]

[a]Cornell High Energy Synchrotron Source, Cornell University, Ithaca, NY 14853, USA, and [b]School of Applied and Engineering Physics, Cornell University, Ithaca, NY 14853, USA. E-mail: rhuang@anl.gov

Single-bounce hollow glass capillaries with ellipsoidal shapes have been used at the Cornell High Energy Synchrotron Source recently for various microbeam experiments, with focal spot sizes from 12 to 23 μm, divergences from 2 to 8 mrad, intensities up to 450 times the intensities of incident X-rays, and working distances up to 55 mm. Simple formulae are developed in this paper to explain capillary performance given the X-ray source size, capillary dimensions and slope errors. Capillary length is optimized for best focusing performance. Capillary fabrication accuracy is reported and capillary X-ray tests confirm the focusing properties expected from formulae. The application of capillaries to third-generation X-ray sources and future energy-recovery linac X-ray sources are discussed.

Keywords: X-ray; focusing; capillary; microbeam; optics.

1. Introduction

Hollow glass capillaries employed at synchrotron radiation sources can be divided into two major categories: polycapillaries, which are fabricated from bundles of many hollow glass fibers and are able to compress X-rays into beam sizes with diameters of tens of micrometers and accept large solid angles subtending many degrees (Kumakhov, 2000; MacDonald & Gibson, 2003; Bjeoumikhov *et al.*, 2003; Ding *et al.*, 1997; Gao *et al.*, 1997); and monocapillaries, which are made of just a single hollow glass tube and can focus X-rays into micrometer and even submicrometer spot sizes (Engström *et al.*, 1991; Riekel *et al.*, 1997; Bilderback, 2003) while subtending generally less than 1° of angular acceptance. There are two further different classes among monocapillaries: multi-bounce capillaries and single-bounce capillaries (SBCs). A multi-bounce capillary focuses X-rays by funnelling them from a larger entrance opening into a smaller tip opening, allowing X-rays to be reflected from the inner wall many times. The capillary tip opening size for the most part determines the spot size, and its figure accuracy can be very approximate, which makes it relatively easier to fabricate for 1 μm and submicrometer focal sizes (Stern *et al.*, 1988; Thiel *et al.*, 1993; Bilderback *et al.*, 1994; Noyan *et al.*, 2000). This type of monocapillary, however, has the disadvantage of a very short (generally less than 1 mm) working distance (the distance from capillary exit tip to the sample) and generally uncontrolled beam divergence, which makes the applications limited. On the other hand, a SBC can focus X-rays with larger working distance, control the maximum X-ray divergence after focusing and has a reflectivity of greater than 95% (Bilderback & Huang, 2001). The X-rays focused by a SBC are suitable for a larger variety of microbeam experiments, which may involve the request of small beam divergence after focusing and a several centimeters range of sample to capillary working distance, such as for cryogenic cooling of protein samples or looking at fluid inclusions in rocks or measuring samples placed in a diamond anvil cell *etc.* However, to make a good quality SBC is a great challenge in glass fabrication. Single-bounce glass capillary applications with a synchrotron source were first introduced by Balaic *et al.* (1995, 1996), and later on followed by developments at Cornell (Bilderback & Fontes, 1997; Bilderback & Huang, 2001) at the Cornell High Energy Synchrotron Source (CHESS). One alternate fabrication method to drawing a glass capillary is electroplating or pressing a metal capillary with a precisely etched metal mandrel (Hirsch, 2000, 2003).

Since our last report of the first 4 mrad capillary X-ray test (Bilderback & Huang, 2001), more progress in SBC development has been made at CHESS. We can now focus X-rays without the larger divergence second bounce that was observed in our last report, which is a critical improvement for all diffraction applications. This improvement was obtained

‡ Current address: IMCA-CAT/CARS, University of Chicago, c/o Advanced Photon Source, Argonne National Laboratory, 9700 South Cass Avenue, Argonne, IL 60439, USA. Email: rhuang@anl.gov.

mainly by making the capillary length equal to twice the focal distance, which is the optimized length for best focusing as discussed in this paper. With further refinements of the glass puller control system, capillary profile accuracy has also been significantly improved, enabling us to make dozens of capillaries with total divergence controlled very well at various values (from 2 to 8 mrad) for a variety of applications at CHESS, such as microcrystallography, microbeam X-ray standing wave (Kazimirov *et al.*, 2004), scanning microspectroscopy (Bilderback *et al.*, 2002), microbeam high-temperature high-pressure diffraction with diamond anvil cells and confocal X-ray fluorescence (Woll *et al.*, 2005). Optical formulae are developed below to easily explain SBC focusing properties even without numerical coding, which helps both beamline scientists and users to choose capillary parameters to best fit their applications.

In this paper we first briefly describe the SBC fabrication accuracy at CHESS, followed by the description of the capillary formulae we developed and some considerations about SBC design. Several examples of capillary X-ray tests are in excellent agreement with the optical formulae. A brief discussion of the potential of using the capillaries for third-generation synchrotron sources and future energy-recovery linac (ERL) sources are given at the end of this paper.

2. Capillary fabrication accuracy at CHESS

The capillary pulling process starts by heating a small section of a straight uniform glass tube with an electric furnace. By accurately controlling the glass extension and heating-zone parameters, we can produce a capillary with ellipsoidal figure (Bilderback & Fontes, 1997). Further, by rotating the tube during pulling, we can keep the pulled capillary centerline straight. The capillary outer profiles are measured under a light microscope with an encoded *xy* stage sample holder, and the inner profiles are calculated from the outer profiles by scaling the ratio between the tubing inner diameter (ID) and outer diameter (OD). Because of the *xy* stage accuracy limits and the microscope image reading accuracy limit, the accuracies of these measurements are presently about 1–2 μm. Two capillary profiles are shown in Fig. 1, with their OD RMS deviations (∼2 μm) from ideal profiles and centerline maximum deflections (∼±1 μm) from straight lines both close to the measurement accuracy limit of our equipment. The capillary ID profile errors will be smaller by a factor of OD/ID if this ratio is constant along a capillary as we assumed. To our knowledge these capillaries have probably the highest optic accuracy so far: they are apparently better than those single-bounce glass capillaries reported earlier (Bilderback &

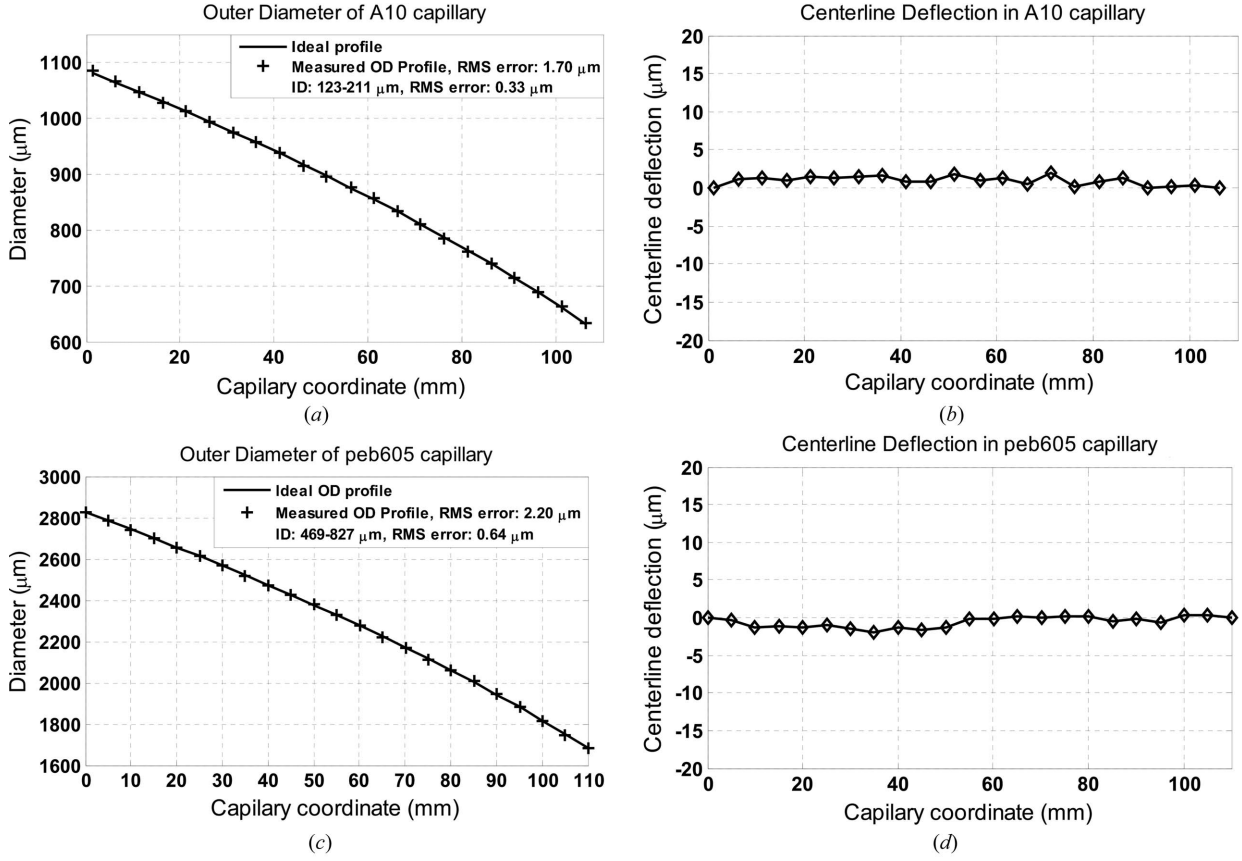

Figure 1
(*a*), (*b*) Capillary OD profile and centerline straightness *versus* capillary length of a 2 mrad capillary measured with a visible-light microscope. The measured OD figure RMS error after subtracting the ideal ellipsoidal profile is 1.7 μm; the maximum centerline deviation is about 2 μm (or ±1 μm); the calculated ID figure RMS error is 0.33 μm assuming that the OD/ID ratio is constant along the capillary. (*c*), (*d*) 8 mrad capillary OD profile and centerline straightness, with measured OD RMS error of 2.2 μm (and a calculated ID profile RMS error of 0.64 μm after scaling down with the OD/ID ratio), and a centerline straightness maximum deflection of ∼2 μm.

Huang, 2001; Bilderback & Fontes, 1997; Balaic *et al.*, 1995) and are also straighter than the electroplated capillaries made from precisely etched metal mandrels whose deviations from straight lines are less than ±10 µm on their good optics (Hirsch, 2003). In general, small optical surface slope errors mean good optical quality and in the following sections we will use the average slope errors to quantify our capillary focusing property. If we simply use the measured OD profiles to calculate the capillary inner surface optic quality, the RMS slope errors of the A10 capillary (Figs. 1*a* and 1*b*), for instance, will be about 72 µrad (26 µrad from diameter error and 68 µrad from straightness error), and the RMS slope errors of the Peb605 capillary (Figs. 1*c* and 1*d*) will be about 88 µrad (53 µrad from diameter error and 70 µrad from straightness error). These values are fairly approximate because of the limited accuracy of the present measurements. Later on, however, we will find out that the actual capillary slope errors obtained from X-ray tests are approximately consistent with these numbers.

3. Capillary focusing calculation

Since the early stage of capillary application, researchers have been using ray-tracing to calculate capillary transmission (Furuta *et al.*, 1993) and focusing profiles (Xiao *et al.*, 1992; Voss *et al.*, 1994; Chen *et al.*, 1994; Vincze *et al.*, 1995; Thiel, 1998) to explain capillary performance (Wang *et al.*, 1996; Vincze *et al.*, 1998) and to optimize the capillary design (Vincze & Riekel, 2003; Gao & Ponomarev, 2003). In this section we introduce some simple formulae that are simplified from our previous work (Huang & Bilderback, 2001) to easily calculate SBC focusing properties and optimize capillary designs without using the complexity of a full three-dimensional ray-tracing program. The formulae have now been embedded in a *Matlab* program that is available on-line (Huang, 2005) and is simple enough to use that even ordinary users of one-bounce glass capillary optics can simply change the capillary input parameters and quickly predict the focal spot size and intensity gain. In normal cases, this eliminates the need to run the more fully featured code in the above ray-tracing programs.

We employ the following terminology in this paper: source spectral brightness is the X-ray radiation intensity per unit source area per unit solid angle. The X-ray focusing intensity profile, or flux profile, is the spatial profile of X-ray flux per unit area after focusing. The X-ray intensity gain, or flux gain, is the ratio of X-ray flux per unit area with a capillary to the X-ray flux per unit area without a capillary. The maximum X-ray intensity gain with a capillary occurs at the center of the focused spot.

3.1. Formulae for capillary focusing profile calculation

The basics of an ellipsoidal SBC focusing can be understood from Fig. 2, where the capillary is ellipsoidal in shape. X-rays emitted from one focus will reach another focus by a single reflection. The X-rays reflected from the tip of the capillary make the maximum divergence of the beam after focusing. This maximum divergence is decided, during the design process, by either the capillary material maximum total reflection angle or the maximum divergence allowed by the application itself. For an X-ray source with non-zero size around the source focus, it will make a non-zero image around the other focus. The fundamental formulae for ellipsoidal mirror focusing were given a long time ago (Howell & Horowitz, 1975; Voss *et al.*, 1992). For capillary applications with a synchrotron source, it can be assumed that both the source and image are small and are on the planes, called the source and image planes respectively in this paper, which pass through the foci and are perpendicular to the major axis. Under these assumptions it is convenient to start the focusing calculation using the formula that relates the source (s) to image (i) position by (Huang & Bilderback, 2001),

$$\begin{aligned} r_\mathrm{i} &= M r_\mathrm{s}, \\ \theta_\mathrm{i} &= \pi - (\theta_\mathrm{s} - 2\phi), \end{aligned} \tag{1}$$

where $(r_\mathrm{s}, \theta_\mathrm{s})$, $(r_\mathrm{i}, \theta_\mathrm{i})$ are the coordinates in the source and image planes, as shown in Fig. 3, and ϕ is the azimuth angle at the capillary inner surface where X-rays are reflected, $M = F_2/F_1$ is the magnification factor, F_1 is the source distance, and F_2 is the image distance. It is obvious that at an image position $(r_\mathrm{i}, \theta_\mathrm{i})$, the X-rays with different propagation directions come

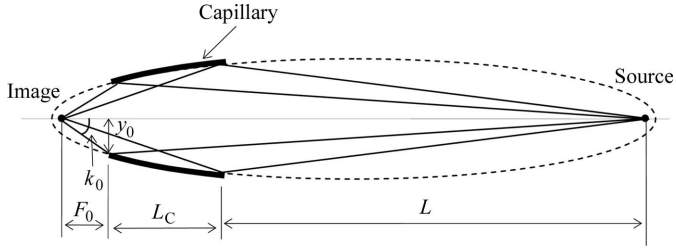

Figure 2
With a single-bounce ellipsoidal capillary, X-rays emitted from one focus (the source) will be reflected into another focus (the image) by just one bounce. For application with a synchrotron source, it is assumed that F_0, $L_C \ll L$, where F_0 is the focal distance, L_C is the capillary length and L is the source distance. The capillary tip opening is $2y_0$, and the X-ray maximum divergence after focusing is $2k_0$.

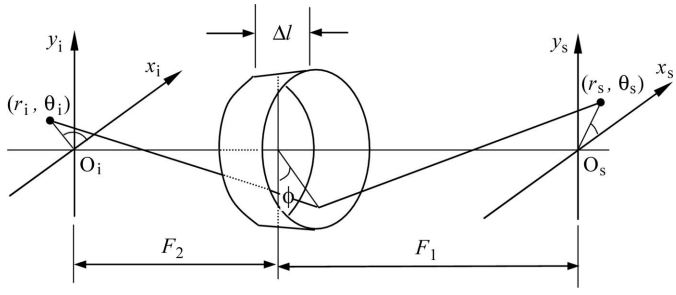

Figure 3
With O_i and O_s as the two foci of the ellipsoid upon which the reflection surface sits, an X-ray from an off-axis point source at $(r_\mathrm{s}, \theta_\mathrm{s})$ on one focal plane is reflected from the ellipsoidal surface at azimuth angle position ϕ, and reaches an off-axis image position $(r_\mathrm{i}, \theta_\mathrm{i})$ of the other focal plane. These three points are related by equation (1) in this paper.

from different parts of the source with reflections at different azimuth angles ϕ of the capillary. Therefore, unless we are dealing with a uniform source, the image spectral brightness should be propagation-direction dependent, *i.e.* $B_i = B_i(r_i, \theta_i, \phi)$. We use the capillary azimuth angle ϕ as the image propagation-direction variable for mathematical convenience. For a SBC working at a reflection angle less than its critical angle, the X-ray reflectivity can be approximated to be unity (Bilderback & Huang, 2001). The X-ray flux at the image position of (r_i, θ_i) coming from a section of capillary with very short length Δl (Fig. 3) will then be

$$\Delta F_i(r_i, \theta_i) = \left(2\pi b^2/a\right)\left(\Delta l/F_2^2\right)\bar{B}_s(r_i/M), \qquad (2)$$

where a and b are the major and minor semi-axes of the capillary inner surface ellipsoid and $\bar{B}_s(r_i/M) = \bar{B}_s(r_s)$ is the angular average of the source spectral brightness. For simplicity of discussion, let us assume that the angular average of the synchrotron source can be approximately given by

$$\bar{B}_s(r_s) = B_0 \exp\left(-r_s^2/\delta_a^2\right), \qquad (3)$$

where $\delta_a = (\delta_x\delta_y)^{1/2}$ if the source is not perfectly round, with a spectral brightness of $B_0 \exp(-x^2/\delta_x^2)\exp(-y^2/\delta_y^2)$. (Later on we will find out that this has to be modified for a very flat synchrotron source.) We also assume that the slope error will blur each unit intensity point image at the position (R_i, φ_i) at the image plane into a Gaussian distribution around this point,

$$E(x_i, X_i, y_i, Y_i) = \frac{1}{\pi(\alpha F_2)^2} \times \exp\left\{-\left[\left(\frac{x_i - X_i}{\alpha F_2}\right)^2 + \left(\frac{y_i - Y_i}{\alpha F_2}\right)^2\right]\right\}, \qquad (4)$$

where $x_i = r_i\cos\theta_i$, $y_i = r_i\sin\theta_i$, $X_i = R_i\cos\varphi_i$, $Y_i = R_i\sin\varphi_i$ and α is the angle of average slope errors. Convoluting (2) with (4) gives us the image profile from a very short section of capillary. Integrating the convoluted result over the whole length of a capillary, and then dividing it by the flux density without a capillary, which is $\pi B_0\delta_x\delta_y/L^2$, we can obtain the flux gain by a capillary. Under the approximation of $a \gg b$, and $F_1 \gg F_2$, and after some simplifications the capillary focal intensity gain can be given by

$$G(r_i) = \left(k_0^2F_0^2/r_0^2\right)\int_{1/(1+L_R)}^{1} \exp\left[\left(-r_i^2/r_0^2\right)t^2\right]\mathrm{d}t, \qquad (5)$$

where

$$\begin{aligned} k_0 &= y_0/F_0, \\ r_0^2 &= F_0^2\left(\delta_a^2/L^2 + \alpha^2\right), \\ L_R &= L_C/F_0. \end{aligned} \qquad (6)$$

As shown in Fig. 2, k_0 is the half-maximum divergence of the X-rays after focusing and y_0 is the radius of the capillary tip opening. L_C is the capillary length, L is the source distance and F_0 is the distance between capillary tip and focal spot (called the working distance). r_0 includes the contributions from both source size and slope errors and is proportional to the final image size.

For most synchrotron sources, however, the flat pancake-shaped source will make the angular averaged profile deviate from a Gaussian shape, as shown in Fig. 4(*a*), especially for a horizontal-to-vertical size ratio larger than 4. In that case, we

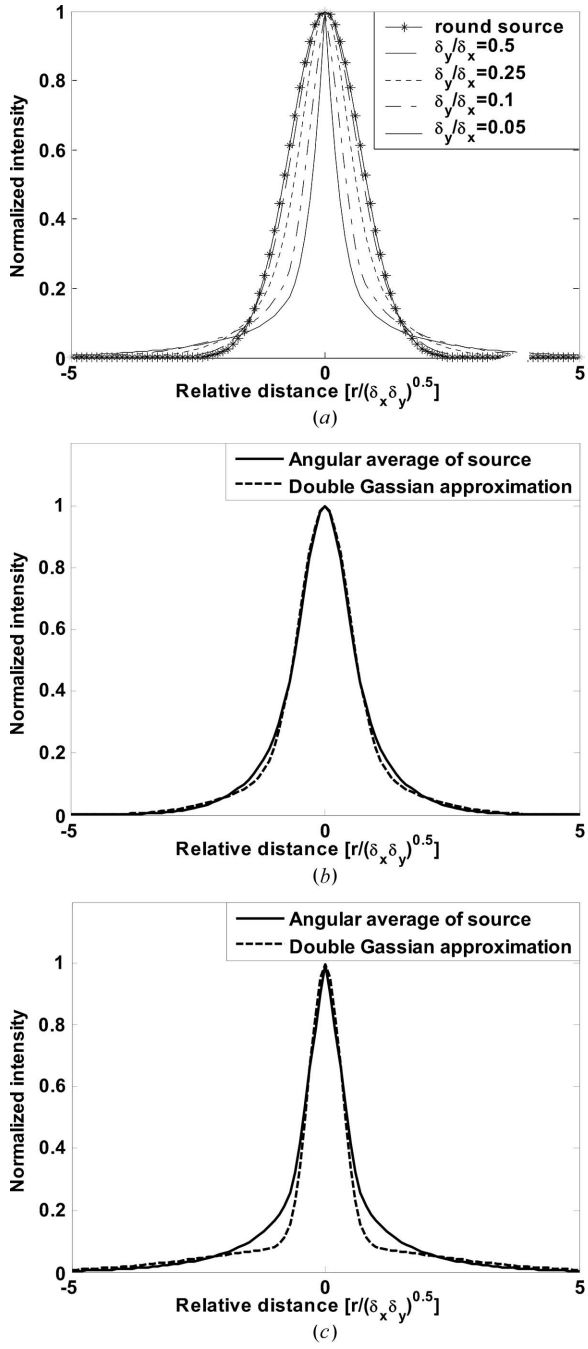

Figure 4
(*a*) Normalized focusing profiles from an infinitely-short capillary of the various flatness sources. For all the sources with the same cross-section area [same $\delta_x\delta_y$ for profile of $\exp(-x^2/\delta_x^2)\exp(-y^2/\delta_y^2)$], as the flatness increases (δ_y/δ_x decreases), the profile will deviate away from Gaussian with a narrow FWHM at the profile center but more X-rays at the wings. (*b*) The double Gaussian approximation agrees with the angular averaged profile for a source with δ_y/δ_x as small as 0.25, but starts to show a clear difference when the source is as flat as $\delta_y/\delta_x = 0.1$, as shown in (*c*).

use a double-Gaussian formula to approximate the angular averaged profile (assume $\delta_x > \delta_y$),

$$\bar{B}_s(r_s)/B_0 = (1-f_0)\exp\left[-(r_s/\delta_m)^2\right] + f_0\exp\left[-(r_s/\delta_n)^2\right], \quad (7)$$

where $\delta_m = 2^{1/2}\delta_x\delta_y/(\delta_x^2+\delta_y^2)^{1/2}$, $\delta_n = \delta_x$ and $f_0 = \delta_y(\delta_x-\delta_y)/[\delta_x(\delta_x+\delta_y)]$. It can be proved that $\exp[-(r_s/\delta_m)^2]$ and $\exp[-(r_s/\delta_n)^2]$ just represent the angular-averaged profile shape of the source around $r_s = 0$ and $r_s = \pm\infty$, respectively. The total photons emitted from the source given by (7) equals the total photons emitted from the profile of $\exp[-(x/\delta_x)^2]$ $\exp[-(x/\delta_y)^2]$. This double Gaussian formula, (7), agrees with the angular-averaged profile very well for $\delta_y/\delta_x \geq 0.25$ (Fig. 4*b*) but not so very well when $\delta_y/\delta_x < 0.1$ (Fig. 4*c*). However, it will be seen below that this approximation is good enough for the current capillary focusing calculation at CHESS, even for the CHESS B2 station, whose source ratio δ_y/δ_x is as small as 0.068. With (7) we can calculate the X-ray intensity gain of using a capillary by

$$G(r_i) = \frac{k_0^2L^2}{\delta_x\delta_y}\frac{L_R}{1+L_R}\left[(1-f_0)k_mS\left(L_R,\frac{r_i}{r_m}\right)+f_0k_nS\left(L_R,\frac{r_i}{r_n}\right)\right], \quad (8)$$

where

$$k_j = \frac{\delta_j^2}{\delta_j^2+(\alpha L)^2} = \frac{1}{1+(\alpha L/\delta_j)^2} \quad (9)$$

with $j = m$ or n and

$$r_j = \left(\delta_j^2M^2+\alpha^2F_0^2\right)^{1/2} = \left(\delta_j/k_j^{1/2}\right)(F_0/L), \quad (10)$$

$$S\left(L_R, r_i/r_j\right) = \frac{1+L_R}{L_R}\int_{1/(1+L_R)}^{1}\exp\left\{-\left[(r_i/r_j)t\right]^2\right\}\mathrm{d}t. \quad (11)$$

Equation (8) suggests that the capillary focal profile will be represented by a summation of two different-sized profiles, with subscription of m and n. k_j gives the slope error effect on the flux gain for each profile; r_j combines both the source size and slope error contributions to the spot size of each profile and $S(L_R, r_i/r_j)$ gives the normalized shape of each one. Depending on the source shape (the δ_y/δ_x ratio), the image of a Gaussian source after capillary focusing can be estimated either by (5) or (8). Both approaches are much simpler than ray-tracing or our previous coding method (Huang & Bilderback, 2001). Actually, by using a mathematical table of the error function, the integrations (and therefore the focal profiles) can even be calculated without coding. For example, the integration of (11) can be easily calculated from the error function

$$S\left(L_R, r_i/r_j\right) = \frac{1+L_R}{L_R}\frac{\pi^{1/2}}{2}\frac{r_j}{r_i}\left\{\mathrm{erf}\left(\frac{r_i}{r_j}\right)-\mathrm{erf}\left[\frac{r_i}{r_j(1+L_R)}\right]\right\}, \quad (12)$$

and remember $S(L_R, 0) = 1$, which is an obvious result from (11). A similar expression can be obtained from (5) for a round source,

$$G(r_i) = \frac{k_0^2F_0^2}{r_0^2}\frac{\pi^{1/2}}{2}\frac{r_0}{r_i}\left\{\mathrm{erf}\left(\frac{r_i}{r_0}\right)-\mathrm{erf}\left[\frac{r_i}{r_0(1+L_R)}\right]\right\}. \quad (13)$$

3.2. Consideration of capillary design

3.2.1. Capillary focusing quality *versus* capillary length. In order to collect more photons into a focal spot, designers used to make very long capillaries, such as capillaries as long as 240–300 mm with a 25–45 mm focal distance (Balaic *et al.*, 1995; Bilderback & Huang, 2001). However, the above formulae suggest that a very long SBC will focus X-rays with a lower percentage of photons in the spot center and more photons in the spot outer area, which is not an ideal situation for most microbeam experiments. For a round source, the normalized image profile from a capillary can be obtained by the integration

$$S(L_R, r_i/r_0) = \frac{1+L_R}{L_R}\int_{1/(1+L_R)}^{1}\exp\left\{-\left[(r_i/r_0)t\right]^2\right\}\mathrm{d}t, \quad (14)$$

where $L_R = L_C/F_0$ (*i.e.* capillary length over focal distance) and we call it the relative capillary length, and r_0 is given by (6). For a flat source, the final focal spot is calculated with the summation of two profiles of different sizes [equation (8)], and both of them are similar to (14) except for the substitution of r_0 with r_m and r_n. Therefore, without losing generality, we can use (14) to discuss the capillary focusing quality with examples of relative lengths of 1 and 8, as shown in Fig. 5(*a*). While the $L_R = 1$ capillary focal intensity profile is close to Gaussian, the profile from a $L_R = 8$ capillary deviates away from the Gaussian shape with long tails at the wings of the profile. For an ideal two-dimensional Gaussian intensity profile, there will be 50% of the total photons within a diameter equal to the FWHM, and 80% of total photons within a diameter equal to 1.52 times the FWHM area. For the sake of discussion, let us temporarily call those diameters the spot sizes. Increasing the capillary length will make these spot sizes larger (Fig. 5*b*) because of the increased photon density within the outer image area. From this point of view, the shorter a capillary is, the better the focusing will be.

3.2.2. Maximum X-ray gain *versus* capillary length. A shorter capillary collects fewer photons in total than a longer one because of its smaller reflecting area. What is the best compromise for having both good flux and good focusing quality? The X-ray maximum gain at the image center ($r_i = 0$) can be calculated from (5) [or (8)] as

$$G(0) = \frac{k_0^2F_0^2}{r_0^2}\frac{L_R}{1+L_R}, \quad (15)$$

or

$$G(0) = \frac{k_0^2L^2}{\delta_x\delta_z}\frac{L_R}{1+L_R}\left[(1-f_0)k_m+f_0k_n\right], \quad (16)$$

for a very flat source. In either case, the X-ray intensity gain at the image center is proportional to $L_R/(1+L_R)$, where L_R is

Table 1
Some CHESS SBCs with their names, lengths, inside diameters at capillary bases and tips, working distances (F_0), FWHMs of focal beam sizes, measured maximum flux gain (G_{max}) and maximum beam divergences after focusing.

Capillary name	Length (mm)	Base/tip IDs (μm)	F_0 (mm)	Size (μm)	G_{max}	Divergence (mrad)
BSG2, BSG3	300	400/130	30	18	115	4.0
BSG625, BSG631	105	407/233	55	22	80	4.0
BSG7, BSG301	50	198/125	30	12	90	4.0
A10	105	211/123	55	14–18	70	2.0
Peb605	115	827/469	55	17–23	455	8.0

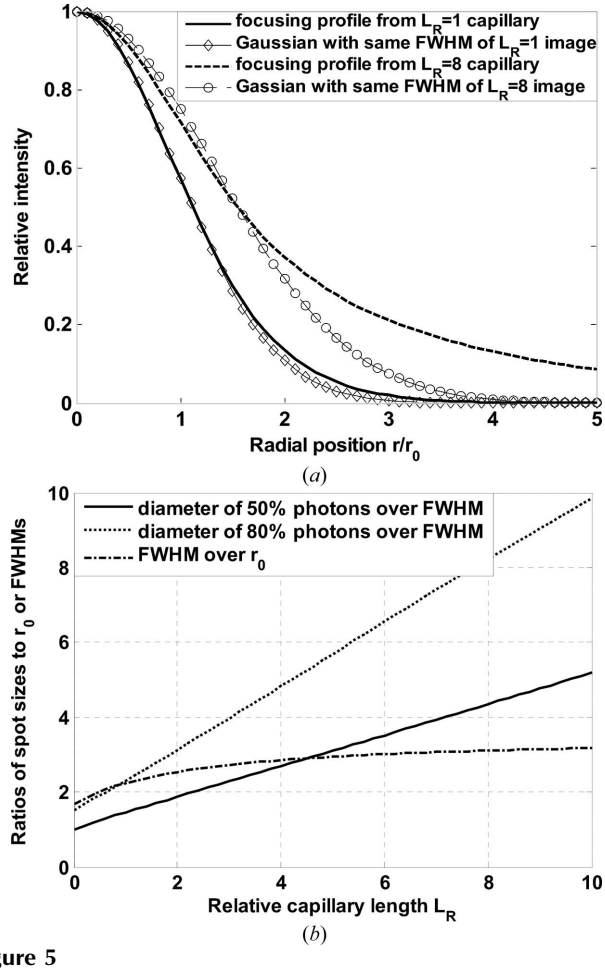

Figure 5
(*a*) The calculated round source ($\delta_x = \delta_y$) focal intensity profiles from two different relative length capillaries, and compared with two ideal Gaussian profiles with the same FWHMs as the focal spots. For the $L_R = 1.0$ capillary the intensity profile is quite close to Gaussian, but for the $L_R = 8$ capillary the intensity profile deviates from Gaussian with more X-rays in the tails. (*b*) Both the ratio of the focal spot FWHM to r_0 (dash-dot line) and the ratio of spot sizes to FWHMs (solid line and dotted line) increase as the capillary relative length increases.

the relative capillary length as explained above. When the capillary relative length, L_R, is small, *e.g.* less then 1, increasing the capillary length will be very necessary to increase the intensity gain. But once L_R is much larger than 1, further increasing the capillary length will not increase the flux gain very much at the image center. In our recent capillary designs, we chose a relative length of $\sim$2. While its flux at the focal center from a $L_R = 2$ capillary is about 75% as large as from a capillary of $L_R = 8$, the focal spot size (enclosing 50% or 80% of total focused X-rays, for example) is only about 0.3 times the spot size of the $L_R = 8$ capillary because of the much better focusing quality (see §3.2.1, or Fig. 5). So $L_R = 2$ is about the best compromise length for a SBC when trying to achieve a small focal spot as well as high flux.

3.2.3. Round source *versus* flat source. Even though SBCs are often called imaging capillaries, these capillaries do not make a point-to-point image of the source; instead they smear the image from one point of a source into an annular ring because of the inherent aberrations of an ellipsoidal mirror (Howell & Horowitz, 1975). This is why we obtain a round focal spot instead of a flat one, even for a pancake-shaped synchrotron source. Because of this angular average focusing effect, a SBC cannot take much advantage of the very small vertical dimension of a flat source as other optics do, such as Kirkpatrick–Baez mirrors. The very flat source may create a focal spot with a profile of small FWHM, but it produces large tails in the focal profile because of the large beam size in the horizontal dimension (Fig. 4*a*). This effect was confirmed with our capillary test at the CHESS B2 station described in the next section of this paper.

3.2.4. Slope errors and source size effect on imaging. It can be seen from either equation (6) (for a round source) or (10) (for a very flat source) that the focal spot size is proportional to $F_0(\delta^2/L^2 + \alpha^2)^{1/2}$, where F_0 is the capillary focal distance, δ is the source dimension, L is the source distance and α is the average slope error. Thus the formulae also suggest that a capillary with large slope errors will blow up the focal spot size and decrease the focusing gain. One of the major reasons why our capillaries are good focusing optics at CHESS is that our capillary slope errors are comparable with, or in some cases even smaller than, the incident X-ray divergence subtending the CHESS source size. Other obvious focusing properties explained by the formulae are: the spot size is proportional to the focal distance; and the flux is proportional to the square of the X-ray divergence after focusing.

4. Summary of single-bounce capillary X-ray tests

Table 1 lists some of the capillaries we made in recent years for the direct focusing of synchrotron radiation. Direct focusing means that there are no other focusing optics in use; otherwise, refer to our recent paper about secondary focusing (Huang & Bilderback, 2003). In this section we use selected examples of SBC X-ray tests at CHESS to demonstrate the SBC focusing properties we discussed above. The focal profiles from these capillaries are measured at the CHESS D1, B2 and A2 stations, and their source parameters at the time of the capillary X-ray tests are listed in Table 2.

4.1. The first 4 mrad capillary at CHESS

The first SBCs made at CHESS with total divergence controlled to 4 mrad are labelled BSG2 and BSG3. The total

Table 2
Source parameters of the CHESS D1, B2 and A2 stations when the capillaries were tested.

Station name	Source–capillary distance (m)	Vertical FWHM (mm)	Horizontal FWHM (mm)
D1	13.3	0.8	2.0
B2	15.0	0.47	6.9
A2	35.0	0.53	4.87

divergence means the maximum X-ray beam divergence from side to side (it is larger than the FWHM divergence, which is sometimes used to rate other focusing optics). These 4 mrad capillaries are 300 mm long, with working distances of 30 mm, and have base and tip inner diameters of 400 and 130 μm, respectively. These capillaries generate a maximum gain of 115 and FWHM of 17 μm (from a vertical scan using a 10 μm pinhole) to 18 μm (horizontal scan). More details of the X-ray test and the numerical simulation of the focal profile were reported previously (Bilderback & Huang, 2001; Huang & Bilderback, 2001). Here the focal profile is compared with the calculation using equation (13), with slope errors of 0.145 mrad, and they agree very well with each other (Fig. 6). It can be seen from Fig. 4(*a*) that for a vertical and horizontal source dimension ratio of ∼0.5 the angular average of the source profile still looks close to Gaussian. Since this ratio is 0.4 for the CHESS D line, the simpler round source formulae can be used for the focusing calculation.

On the other hand, compared with an ideal Gaussian (for example, the round source profile in Fig. 4*a*), the intensity profile from this capillary has a higher percentage of X-rays at the outer wings because of the large relative capillary length (10 for capillary BSG2). Meanwhile there was a secondary reflection problem with this capillary (Bilderback & Huang, 2001). Because of slope errors, a small fraction of the reflected X-rays are so far away from the focused point that they hit the capillary inner wall on a second bounce before escaping from the capillary. These secondary reflected X-rays have divergences larger than the design of 4 mrad, but can mainly be eliminated with a 40 μm aperture near the focus. A better solution, however, is to eliminate the second bounce opportunity by improving capillary quality and shortening the capillary length to a more reasonable value as discussed below.

4.2. 4 mrad divergence capillaries with shorter relative length

To improve the intensity profile after focusing and meanwhile to avoid the double-bounce problem mentioned above, we designed two other 4 mrad capillaries with reduced capillary length. One design, with capillaries named as BSG625 and BSG631, has their entrance diameter of 407 μm close to the entrance diameter of the BSG2 capillary, but with a working distance of 58 mm (experimental value around 55 mm) and a capillary length of 105 mm. The X-ray accepting area (the tip opening area subtracted from the entrance area) of the BSG625 capillary is about 78% of the BSG2 accepting area. Experimentally we measured the maximum flux gain at the image center of about 80, 70% as large as the BSG2 capillary, and spot FWHM of 21 (vertical scan) to 22.3 μm (horizontal scan), with the FWHM area 50% more than the BSG2 capillary (Fig. 7). Therefore this shorter capillary focuses slightly more photons into its FWHM area than the BSG2 capillary even as it intercepts fewer total X-rays, leaving less percentage of X-rays in the outer area of focus. Because of the larger tip opening and shorter capillary length, there were no secondary reflections found from this capillary. The pedestal within the position of the ±115 μm area in Fig. 7 is the direct beam through the capillary tip opening and can be stopped by a beam block upstream of the capillary.

Another 4 mrad capillary, BSG7, was made with the same focal distance and tip opening as the BSG2 capillary, but with its relative length reduced from 10 to 1.67. With its base

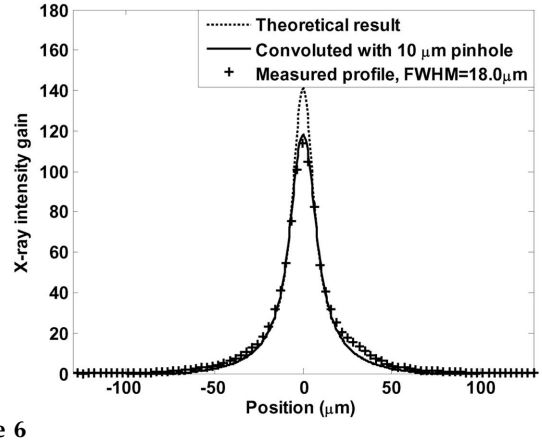

Figure 6
The measured focal spot of our first 4 mrad capillary at the CHESS D station, with a FWHM of 18 μm and a maximum gain of 115 while checked with 10 μm pinhole scan, matches the calculated profile, which suggests a FWHM of 18 μm and maximum gain of 120 after 10 μm pinhole convolution (solid line), or maximum gain of 141 without convolution (dotted line).

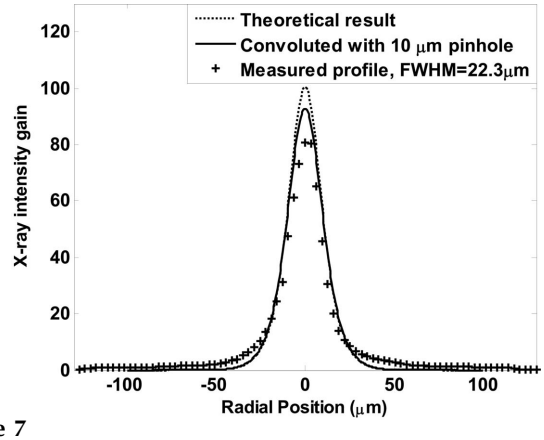

Figure 7
The measured intensity profile from the BSG625 capillary (crosses, taken with 10 μm pinhole scan) at the CHESS D station is close to the calculated profile with slope errors of 0.145 mrad (dots, without convolution and solid line after 10 μm pinhole convolution). Compared with the BSG2 capillary, this shorter relative length capillary has a higher percentage of focused X-rays at the spot center area. The pedestal in the measured profile is the direct beam from the 230 μm capillary tip opening, which can be stopped with a beam block upstream of the capillary.

opening diameter of 198 μm, its acceptance area for X-rays is about 17% of the BSG2 capillary. The measured maximum flux gain is about 90, slightly smaller than the measured BSG2 maximum gain of 115. But it gives a smaller focal spot of about 11.6 μm and has a much better focused profile with far fewer X-rays in the spot tails. In Fig. 6 the profile tails of the BSG2 capillary extend up to 50 μm from center, but in Fig. 8 the profile tails of the BSG7 capillary almost completely disappear by the 20 μm position. The pedestals in Fig. 8 with intensity around 1, from the −60 μm position to 60 μm, are the X-rays that go through directly from the capillary 125 μm opening without being reflected, but can be stopped with a 125 μm beam block upstream of the capillary. When this capillary was used for a microbeam standing-wave experiment at CHESS with the through-beam blocked, the spatial resolution was once again confirmed to be ∼10 μm by a thin-layer straight-edge fluorescence scan (Kazimirov *et al.*, 2004), close to our measured FWHM.

In conclusion, the best focus with good central flux and small tails occurs for a relative capillary length of ∼2. Shortening the relative capillary length makes the focal intensity profile closer to Gaussian.

4.3. Capillary focusing of a very flat source

It was pointed out earlier that a capillary does not focus a flat source as well as it does for a round source, and this is exactly the case for the CHESS B2 source, with a horizontal FWHM of 6.9 mm and a vertical FWHM of 0.47 mm. The source-to-station distance is 15000 mm, close to the CHESS D line source distance of 13300 mm; therefore the BSG625 capillary can also be used for the B2 station. If the B2 station source was round [and with the same cross-area, *i.e.* $\mathrm{FWHM}_x = \mathrm{FWHM}_z = (6.9 \times 0.47)^{1/2} = 1.8$ mm], we could expect a focal spot with a maximum gain of ∼97 and a FWHM of ∼24 μm. Instead, however, the measured intensity profile has a maximum gain of ∼35 and FWHM of 31 μm, which is close to the prediction of a maximum gain of 37 with a FWHM of 34 μm as given by flat source formulae (Fig. 9). Meanwhile, compared with a round source, the flat source focal intensity profile has a higher fraction of the X-rays in the profile outer area (*e.g.* the area from 20 to 60 μm from spot center), therefore it is more obviously a non-Gaussian profile. This is caused by the angular averaging effect discussed in §3.1 and seen in Fig. 4(*a*). This is also direct proof that the focused beam intensity profile is influenced not only by capillary slope errors but also by the X-ray source dimensions and shapes. In spite of the larger horizontal B-line source, this capillary was successfully used at the B1 and B2 stations for high-pressure diffraction experiments, with a beam block to stop the straight-through X-rays, which is the pedestal in Fig. 9 within the ±115 μm area.

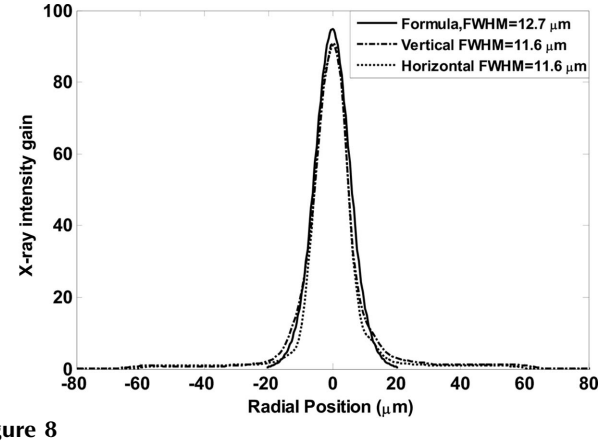

Figure 8
The intensity profiles of another shorter relative length capillary (BSG7) tested at the CHESS D line. With slope errors of 0.125 mrad, the calculated maximum gain and FWHM, after 10 μm pinhole convolution (solid line), are 95 and 12.7 μm, respectively (132 and 10 μm before convolution), close to measured values (91 and 11.6 μm) from the scanning of a 10 μm pinhole (dash-dot and dotted lines). Compared with Fig. 6, this focused X-ray intensity profile is closer to Gaussian with a higher percentage of X-rays within the central peak. The 125 μm-diameter pedestal in the figure comes from the direct X-rays passing through the capillary tip opening and can be stopped with a beam block (not present for this measurement).

4.4. 2 mrad capillary for the A2 station

The maximum divergence of the X-rays after focusing determines the design of a SBC tip opening with $2y_0 = 2k_0F_0$, where $2k_0$ is the maximum divergence after focusing, F_0 is the working distance (Fig. 2) and $2y_0$ is the SBC tip ID. Decreasing the maximum focusing divergence will decrease the capillary tip opening and the diameter of the whole capillary. Consequently, X-rays may more likely be reflected more than once before they leave the capillary if the slope errors are large. So it is more challenging to make low-divergence capillaries. At CHESS we have successfully made a capillary with 2 mrad total divergence with an observed maximum gain of ∼70 at the spot center and a FWHM size of ∼14 μm (vertical) to 18 μm (horizontal) as observed through the scanning of a 10 μm pinhole (Fig. 10). By checking the X-ray spot size far downstream of the capillary focal point, a 2 mrad designed divergence was confirmed. No secondary reflections were

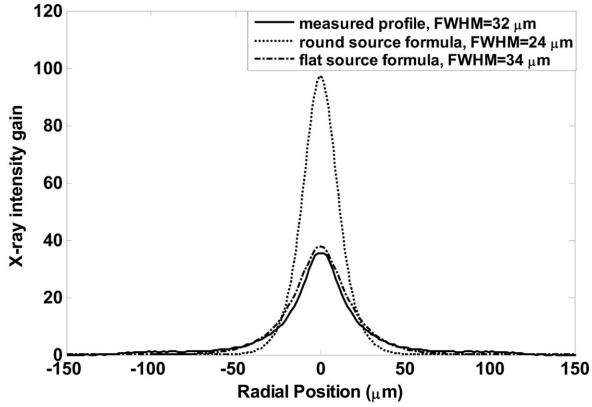

Figure 9
The measured focal profile of the BSG625 capillary used for a flat source, CHESS B2 station, has smaller gain, larger FWHM, and is less likely a Gaussian with more X-rays in the profile wings compared with a calculated focusing of a round source of the same cross-area (dotted line). This measurement can be explained by a flat source formula, equation (8), in the dash-dot line.

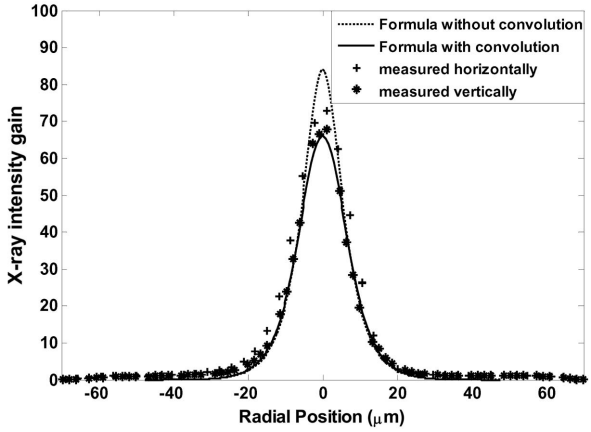

Figure 10
The measured intensity gain from the A10 capillary (the smallest divergent capillary we have made so far) is consistent with slope errors as low as 60 μrad. After 10 μm pinhole convolution, the calculation gives a FWHM of 15 μm and maximum gain of 66 (12.5 μm FWHM and 84 maximum gain without convolution), close to the measured data (see text). The pedestal in the measured profile is the direct beam through the 123 μm tip opening.

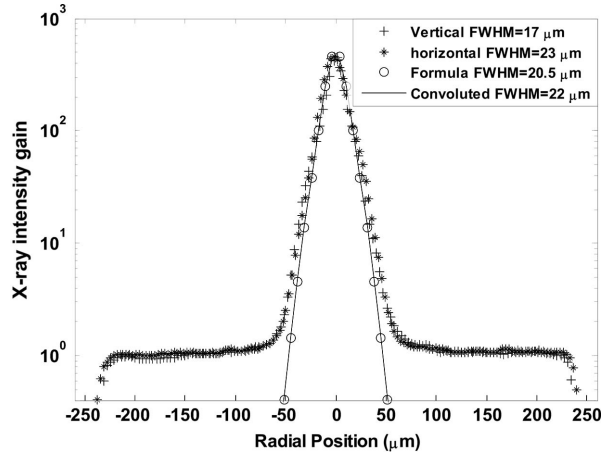

Figure 11
The measured maximum flux gain from an 8 mrad capillary, Peb605, at the CHESS D station is about 455 in both the vertical and horizontal pinhole scans, close to the calculated gain of 460 with pinhole convolution, and 503 without pinhole convolution, with capillary slope errors of 130 μrad. With intensity plotted on a logarithmic scale, the focusing quality is more easily evaluated around the spot tails. The pedestal is the direct beam through the 470 μm tip opening.

observed. This excellent result was due to the very good capillary figure accuracy [of 1–2 μm, see Figs. 1(*a*) and 1(*b*)] and therefore very small slope errors (∼60 μrad from an X-ray test) and a shortening of the capillary relative length to close to 2. The CHESS A2 station has a 24-pole wiggler source with flat dimensions (Table 2). This capillary was designed for potential high-pressure diamond anvil cell diffraction experiments, where there is a need for microbeam X-rays (up to 60 keV), low divergence, several centimeter working distance and high X-ray flux.

4.5. 8 mrad capillary used at CHESS

A larger focused divergence will make a higher flux [equations (5) or (8)]. One good example of this application at CHESS is for fish ear stone (otolith) trace-element X-ray fluorescence (XRF) mapping. Otoliths can record the life history of a fish in much the same way that tree rings record the life history of trees. For this experiment we needed a very high intensity microbeam in order to simultaneously detect multiple trace elements with concentrations down to the PPM range in two-dimensional mapping. Accordingly, we designed a capillary with 8.0 mrad total divergence, 55 mm working distance and 0.827 mm entrance diameter. This capillary focuses the X-rays into a spot of ∼20 μm FWHM, with a maximum intensity gain of ∼455 (Fig. 11). With the CHESS D line bending-magnet source, a 1% multilayer monochromator, and with the accelerator storage ring running at 125 mA, we obtained 1.0×10^{12} X-rays s^{-1} at 10 keV in the full spot after blocking the direct through-beam. This arrangement was successfully used for trace-element microbeam fluorescence mapping (Bilderback *et al.*, 2002), and more recently in a confocal XRF geometry [a monocapillary for focusing the incident beam and a polycapillary at 90° for receiving (Woll *et al.*, 2005)] to obtain an elemental profile along the sample depth direction, similar to the method of Proost *et al.* (2002).

5. Discussion

5.1. SBCs at CHESS

Capillaries are in general use at several CHESS stations for various kinds of experiments. An advantage of using a capillary is that it takes up very little space, and is easy to mount and align without interference to the optical design of the existing station. The divergence can be controlled very well by proper capillary design. Meanwhile, present capillary optical quality is a good match given the current CHESS source size: the incoming X-ray divergence owing to the source size is in the same range as the capillary slope errors. For example, at the CHESS D1 station, with a size (FWHMs) of 2 mm × 0.8 mm, the source at a 13 m distance subtends divergences of 154 μrad (H) and 60 μrad (V), close to the capillary slope errors which are in the range from 60 μrad (A10 capillary) to 145 μrad (BSG625 capillary). Taking a 4 mrad capillary with a 30 mm focal distance for example, Figs. (12*a*) and (12*b*) show the effect of capillary slope errors on the focusing quality. With our current capillary average slope errors of 60–145 μrad, the intensity gain and the spot size are close to the best numbers achievable with the CHESS source. This is especially true for the CHESS B2 station. When slope errors are smaller than 100 μrad, the increased maximum gain at the focal spot center for the B2 station is caused by the very small vertical dimension of the very flat source. This increase comes with a sharp peak only near the center spot area but without changing the X-ray intensity in the wings [see the $\delta_y/\delta_x \ll 1$ profiles in Fig. 4(*a*) or the double Gaussian profile in Fig. 4(*c*)]; therefore there is not much change in the spot size within which a given percentage (*e.g.* 50% in Fig. 12*b*) of X-rays are focused.

On the other hand, at such stations as A2, where the incident X-ray divergence subtending the source size is smaller, there will be a more significant benefit from the improvement

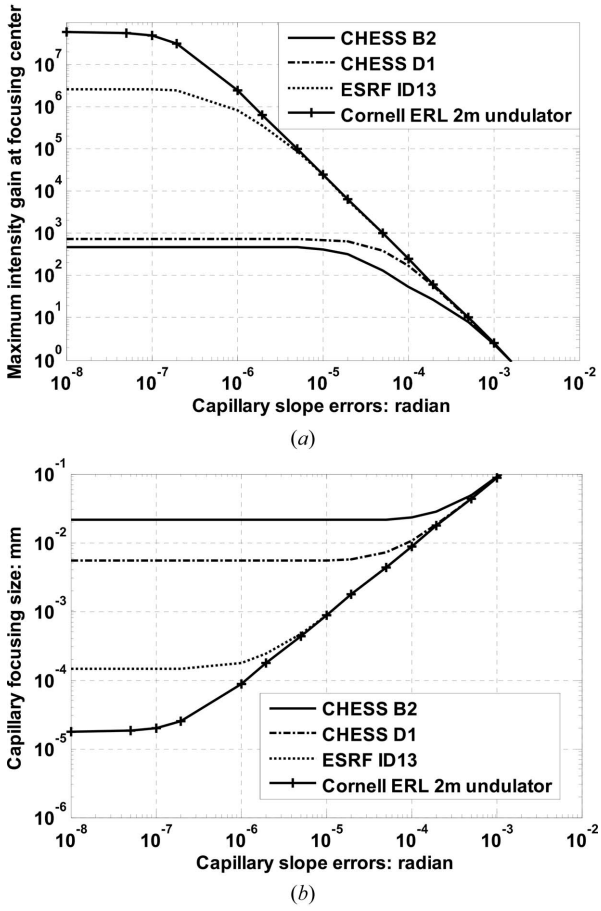

Figure 12
Calculated (*a*) maximum flux gains and (*b*) capillary beam sizes of several different sources, against the capillary slope errors for a capillary of 30 mm focal distance and relative length of 1.7. The parameters used in the calculations are assumed to be: ESRF ID13 ($FWHM_x$ = 123 μm, $FWHM_z$ = 23 μm, source–image distance of 34 m); Cornell ERL 2 m undulator ($FWHM_x = FWHM_z$ = 8.6 μm, source–image distance of 25 m); CHESS D and B2 parameters can be found in Table 2. The 20 nm focal spot of the ERL source, which is close to the 10 nm diffraction limit, should be checked with wave theory for more accurate calculations.

of capillary quality, especially when the CHESS source size becomes smaller in future dedicated operations.

We recently designed and fabricated a 4 mrad capillary with 50 mm working distance for HASYLAB beamline L. Based on the HASYLAB source dimensions and the good quality of that capillary, we predicted with our formulae that the image size could be as small as 11 μm and the maximum intensity gain could be more than 300 when we delivered the capillary. These figures were recently confirmed by X-ray tests of this capillary at HASYLAB (Falkenberg *et al.*, 2003; Schmidt *et al.*, 2003).

5.2. SBC for third-generation sources and ERL sources

Fig. 12(*b*) suggests that with a capillary of current best quality (60 μrad slope error) it may be possible to directly focus an ESRF source into a 5 μm spot with a working distance as large as 30 mm. Reducing the working distance will reduce the focused size in proportion. However, making a capillary with working distance shorter than 15–20 mm, and meanwhile keeping small slope errors, is still a challenge for us at present. Compared with the multi-bounce capillaries currently used at the ESRF (Engström & Riekel, 1996*a*; Riekel *et al.*, 1997), a SBC will have the advantage of a larger working distance, controlled maximum beam divergence, higher X-ray throughput, and more likely a lower background because the total reflection from a SBC prevents X-rays from penetrating the glass wall material as they may in the multi-bounce case (Engström & Riekel, 1996*b*; Riekel *et al.*, 2000). On the other hand, current SBCs cannot presently focus a spot as small as 100 nm, which in principle is possible now by using a multi-bounce capillary with the ESRF source (Vincze & Riekel, 2003).

The capillary profiles shown in Fig. 1 are about the best profiles we can obtain with our current equipment, but it may be possible to obtain better in the future with more development work. Fig. 12 also shows that if some new technology allows us someday to make much better capillaries with negligible slope errors and surface roughness, according to our formulae a 20 nm focal spot might be achievable with a 30 mm working distance (or 10 nm spot with 15 mm working distance) for an ERL type of X-ray source (Gruner *et al.*, 2002; a superior radiation source to current storage rings). We are presently not too optimistic that such great improvements can be made with the current glass drawing methods, but this still has to be determined by further fine-tuning the drawing process itself. Since this situation actually approaches the diffraction limit, a wave theory might be needed to correctly calculate capillary focusing in the limits of really small beam size. The maximum total reflection angle, approximated as θ_c [mrad] = 2.7λ [Å] for low-Z materials, and θ_c [mrad] = 6.2λ [Å] for high-Z materials, limits the capillary maximum tip opening (radius) by $y_0 = k_0F_0 = 2\theta_cF_0$ (see Fig. 3, with the assumption of parallel incident X-rays). This limit of capillary opening will impose a minimum spot size, by the Rayleigh criterion, of

$$d = \frac{0.61\lambda}{y_0}F_0 = \frac{0.61\lambda}{2\theta_c} = \frac{0.61\lambda}{2 \times 6.2 \times 10^{-3}\lambda} = 50\ \text{Å}$$

for high-Z material, and 110 Å for low-Z material such as glass. Therefore we do not expect to use a SBC to make X-ray beams down to a scale of 5–10 nm (Bilderback & Huang, 2003). This is just in the range where other fundamental limits in X-ray optical performance may become apparent as recently discussed (Bergemann *et al.*, 2003). The simple formulae developed in this paper, as well as all the ray-tracing methods based on geometric optics, will not correctly predict the focusing under this situation, but should be suitable for beams that are a few times larger than the 10 nm diffraction limit, for perfect capillaries.

6. Summary

In summary, we have developed simple formulae that can predict the capillary performance given the synchrotron source parameters, the capillary figure, and the slope errors

from fabrication; more complex ray-tracing designs are not needed. One firm conclusion derived from the formulae is that the optimal capillary length is about twice the focal length (distance from capillary tip to focus) for the best optical performance. X-ray tests of capillaries at several beamline situations at CHESS are in good agreement with the formulae. Both the capillary figure errors and centerline deflections as measured from capillary OD profiles are in the range of a couple of micrometers, the same as our present metrology accuracy limits. The capillary slope errors are now comparable with the incident X-ray divergence subtending the CHESS source size with actual capillary slope errors ranging from 60 µrad to 140 µrad. Applications of capillaries to a third-generation source and the planned future Cornell ERL source are described. In principle, a perfectly shaped single-bounce capillary of current dimensions can focus the ERL X-rays all the way down to the situation where the X-ray wave theory, which sets a minimum size limit of 10 nm, is needed for more precise calculations.

We thank CHESS staff scientists E. Fontes, C. S. Zha, A. Kazimirov and A. Woll for their help on the capillary X-ray tests on the D1, B2 and A2 stations. This work is based on research conducted at the Cornell High Energy Synchrotron Source (CHESS) which is supported by the National Science Foundation and the National Institutes of Health under award DMR-0225180. We also thank G. Falkenberg and K. Rickers for the X-ray test of our capillary at HASYLAB beamline L.

References

Balaic, D. X., Barnea, Z., Nugent, K. A., Garrett, R. F., Varghese, J., N. & Wilkins, S. W. (1996). *J. Synchrotron Rad.* **3**, 289–295.

Balaic, D. X., Nugent, K. A., Barnea, Z., Garrett, R. & Wilkins, S. W. (1995). *J. Synchrotron Rad.* **2**, 296–299.

Bergemann, C., Keymeulen, H. & Van der Veen, J. F. (2003). *Phys. Rev. Lett.* **91**, 204801-1–4.

Bilderback, D. H. (2003). *X-ray Spectrom.* **32**, 195–207.

Bilderback, D. H. & Fontes, E. (1997). *Synchrotron Radiation Instrumentation: Tenth US National Conference, AIP Conference Proceedings 417*, edited by E. Fontes, pp. 147–155. Melville, NY: AIP Press.

Bilderback, D. H., Hoffman, S. A. & Thiel, D. J. (1994). *Science*, **263**, 201–203.

Bilderback, D. H. & Huang, R. (2001). *Nucl. Instrum. Methods Phys. Res. A*, **467–468**, 970–973.

Bilderback, D. H & Huang, R. (2003). *Synchrotron Radiation Instrumentation: Eighth International Conference on Synchrotron Radiation Instrumentation, AIP Conference Proceedings 705*, edited by T. Warwick *et al.*, pp. 1271–1274. Melville, NY: AIP Press.

Bilderback, D. H., Huang, R., Kazimirov, A., Kriksunov, I. A., Limburg, K. & Fontes, E. (2002). *Adv. X-ray Anal.* **46**, 320–325.

Bjeoumikhov, A., Langhoff, N., Wedell, R., Beloglazov, V., Lebed'ev, N. & Skibina, N. (2003). *X-ray Spectrom.* **2003**, 172–178.

Chen, G. J., Cerrina, F., Voss, K. F., Kim, K. H. & Frederick, C. B. (1994). *Nucl. Instrum. Methods Phys. Res. A*, **347**, 407–411.

Ding, X., He, Y. & Yan, Y. (1997). *X-ray Spectrom.* **26**, 374–379.

Engström, P., Larsson, S., Rindby, A., Buttkewitz, A., Garbe, S., Gaul, G., Knöchel, A. & Lechtenberg, (1991). *Nucl. Instrum. Methods*, A**302**, 547–552.

Engström, P. & Riekel, C. (1996*a*). *J. Synchrotron Rad.* **3**, 97–100.

Engström, P. & Riekel, C. (1996*b*). *Rev. Sci. Instrum.* **67**, 4061–4063.

Falkenberg, G., Rickers, K., Bilderback, D. H. & Huang, R. (2003). *HASYLAB Annual Report 2003.* HASYLAB, Hamburg, Germany.

Furuta, K., Nakayama, Y., Shoji, M., Kaigawa, R., Hanamoto, K., Nakano, H. & Hosokawa, Y. (1993). *Rev. Sci. Instrum.* **64**, 135–142.

Gao, N. & Ponomarev, Y. (2003). *X-ray Spectrom.* **32**, 186–194.

Gao, N., Ponomarev, I. Y., Gibson, W. M. & Carpenter, D. A. (1997). *Appl. Phys. Lett.* **71**, 3441–3443.

Gruner, S., Bilderback, D., Bazarov, I., Finkelstein, K., Krafft, K., Merminga, L., Padamsee, H., Shen, Q., Sinclair, C. & Tigner, M. (2002). *Rev. Sci. Instrum.* **73**, 1402–1406.

Hirsch, G. (2000). *Synchrotron Radiation Instrumentation: Eleventh US National Conference, AIP Conference Proceedings 521*, edited by P. Pianetta, J. Arthur and S. Brennan, pp. 253–257. Melville, NY: AIP Press.

Hirsch, G. (2003). *X-ray Spectrom.* **32**, 229–238.

Howell, J. A. & Horowitz, P. (1975). *Nucl. Instrum. Methods*, **125**, 225–230.

Huang, R. (2005). *Single-bounce capillary focusing calculator*, http://glasscalc.chess.cornell.edu/imageprof.html.

Huang, R. & Bilderback, D. H. (2001). *Nucl. Instrum. Methods Phys. Res. A*, **467–468**, 978–981.

Huang, R. & Bilderback, D. H. (2003). *Synchrotron Radiation Instrumentation: Eighth International Conference on Synchrotron Radiation Instrumentation, AIP Conference Proceedings 705*, edited by T. Warwick *et al.*, pp. 712–715. Melville, NY: AIP Press.

Kazimirov, A., Bilderback, D. H., Huang, R., Sirenko, A. & Ougazzaden, A. (2004). *J. Phys. D*, **37**, L9–L12.

Kumakhov, M. A. (2000). *X-ray Spectrom.* **29**, 343–348.

MacDonald, C. A. & Gibson, W. M. (2003). *X-ray Spectrom.* **32**, 258–268.

Noyan, I. C., Wang, P. C., Kaldor, S. K., Jordan-Sweet, J. L. & Liniger, E. G. (2000). *Rev. Sci. Instrum.* **71**, 1991–2000.

Proost, K., Janssens, K., Vincze, L., Falkenberg, G., Gao, N. & Bly, P. (2002). *HASYLAB Annual Report 2002.* HASYLAB, Hamburg, Germany.

Riekel, C., Burghammer, M. & Muller, M. (2000). *J. Appl. Cryst.* **33**, 421–423.

Riekel, C., Cedola, A., Heidelbach, F. & Wagner, K. (1997). *Macromolecules.* **30**, 1033–1037.

Schmidt, C., Rickers, K., Bilderback, D. H., Huang, R. & Falkenberg, G. (2003). *HASYLAB Annual Report 2003.* HASYLAB, Hamburg, Germany.

Stern, E. A., Kalman, Z., Lewis, A. & Lieberman, K. (1988). *Appl. Opt.* **28**, 5135–5139.

Thiel, D. J. (1998). *J. Synchrotron Rad.* **5**, 820–822.

Thiel, D. J., Bilderback, D. H. & Lewis, A. (1993). *Rev. Sci. Instrum.* **64**, 2872–2878.

Vincze, L., Janssens, K., Adams, F. & Rindby, A. (1995). *X-ray Spectrom.* **24**, 27–37.

Vincze, L., Janssens, K., Adams, F., Rindby, A. & Engström, P. (1998). *Rev. Sci. Instrum.* **69**, 3494–3503.

Vincze, L. & Riekel, C. (2003). *X-ray Spectrom.* **32**, 208–214.

Voss, J., Kunz, C., Moewes, A. & Storjohann, I. (1992). *Rev. Sci. Instrum.* **63**, 569–573.

Voss, K. F., Kim, K. H., Stern, E. A., Brown, F. C. & Heald, S. M. (1994). *Nucl. Instrum. Methods Phys. Res. A*, **347**, 390–396.

Wang, L., Rath, B. K., Gibson, W. M., Kimball, J. C. & MacDonald, C. A. (1996). *J. Appl. Phys.* **80**, 3628–3638.

Woll, A., Bilderback, D. H., Gruner, S., Gao, N., Huang, R., Bisulca, C. & Mass, J. (2005). *Mater. Res. Soc. Symp. Proc.* **852**, 281–290.

Xiao, Q. F., Ponomarov, I., Kolomitsev, A. I. & Kimball, J. C. (1992). *Proc. SPIE*, **1736**, 227–228.